Paper:

Basic Study on Reinforced Concrete Shear Walls Without Boundary Columns Retrofitted by Carbon Fiber Sheets

Tomoya Matsui, Taiki Saito, and Roy Reyna

Department of Architecture and Civil Engineering, Toyohashi University of Technology
1-1 Hibarigaoka, Tenpaku, Toyohashi, Aichi 441-8580, Japan
E-mail: matsui@ace.tut.ac.jp
[Received July 1, 2014; accepted September 6, 2014]

Reinforced concrete (RC) buildings in Peru use low ductility walls, with rectangular cross-sections and reinforced with wire mesh and vertical reinforcement bars at boundary ends, as structural elements. These structural elements have no columns, have small amounts of reinforcing bars and are expected to fail in a brittle manner. In this study, a performance verification test is conducted on the use of carbon fiber sheets (CFS) as a retrofitting method for shear walls without boundary columns. The focus is on retrofitting walls that fail in flexural mode. In other words, although an increase in strength cannot be expected, CFS retrofitting can delay the concrete crushing of the shear wall base that occurs during flexural failure; and the aim is to verify this improvement in deformation performance due to CFS retrofitting. From the test, by retrofitting the RC shear wall without boundary columns with CFS, it was found that post-maximum strength deterioration was more gradual, and deformation performance was improved. And Ultimate limit deformation of specimen which was partially retrofitted at the boundary ends of the wall was larger than that of specimen which was retrofitted over the entire wall span.

Keywords: seismic retrofitting, carbon fiber sheet, reinforced concrete wall, shear wall without boundary columns, static loading test

1. Introduction

Reinforced concrete (RC) buildings in Peru use low ductility walls, with rectangular cross-sections and reinforced with wire mesh and vertical reinforcement bars at boundary ends, as structural elements [1]. These structural elements have no columns, have small amounts of reinforcing bars and are expected to fail in a brittle manner. On the other hand, for RC shear walls without boundary columns, the flexural compression failures in multi-story shear walls during the 2010 Chile Earthquake drew a lot of attention [2] as shown in **Fig. 1**.

In this study, a performance verification test is conducted on the use of carbon fiber sheets (CFS) as a retrofitting method for shear walls without boundary columns such as those mentioned above. Note that there have already been several reports [3] published on the effectiveness of CFS retrofitting on walls failing in shear or on walls with a boundary column on one side. Here, however, the focus is on retrofitting walls that fail in flexural mode. In other words, although an increase in strength cannot be expected, CFS retrofitting can delay the concrete crushing of the shear wall base that occurs during flexural failure; and the aim is to verify this improvement in deformation performance due to CFS retrofitting.

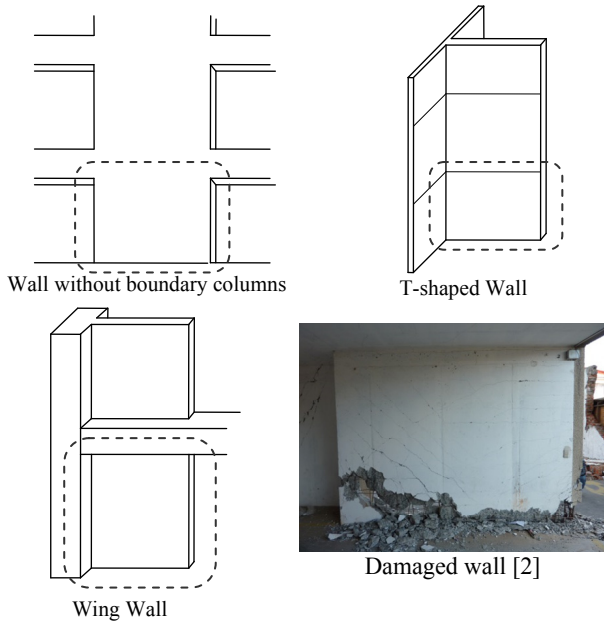

Fig. 1. Type of wall without boundary column.

2. Outline of Loading Test

2.1. Specimens

Tables 1–4 provide the test specimens list and the concrete, reinforcing bars and CFS material properties. **Figs. 2** and **3** show the bar arrangement and schematic diagram of the test specimens. There are a total of three test specimens of RC shear walls without boundary columns. The test variables selected were the presence/absence of

Table 1. Test specimens list.

		WF	RWF1	RWF2
Wall	$l_w \times h_w$ (mm)	1600×1600		
	Wall thickness t_w (mm)	80		
	Vertical reinforcement at boundary ends	3-D13		
	Wall mesh reinforcement	D6@150 single ($p_w = 0.27\%$)		
Retrofit Mode (mm)		Unretrofitted	Over wall span $L = 1600$	Both boundary ends of wall $L = 400$/side

Table 2. Concrete material properties.

Specimen	σ_B (N/mm^2)	E_c (N/mm^2)	ε_{c0} (μ)	f_t (N/mm^2)	Age (days)
WF	33.5	26800	2280	3.0	54
RWF1	35.2	26400	2560	2.9	62
RWF2	29.8	27200	2150	2.9	67

σ_B: Compressive strength, E_c : Modulus of elasticity,
ε_{c0}: Strain at compressive strength, f_t: Tensile strength by split cylinder test

Table 3. Reinforcing steel material properties.

Name (Property)	σ_y (N/mm^2)	σ_u (N/mm^2)	E_s (N/mm^2)	Use
D6 (SD295A)	359	474	174600	Wall mesh reinforcement
D13 (SD295A)	355	516	182100	Vertical reinforcement at bounday ends

σ_y: Yield strength, σ_u: Tensile strength, E_s: Modulus of elasticity

Table 4. CFS material properties.

Fiber weight	g/m^3	300
Sheet thickness	mm	0.167
Density	g/m^3	1.80
Tensile strength	kN/mm^2	3.4
Modulus of elasticity	kN/mm^2	230
Width	mm	330

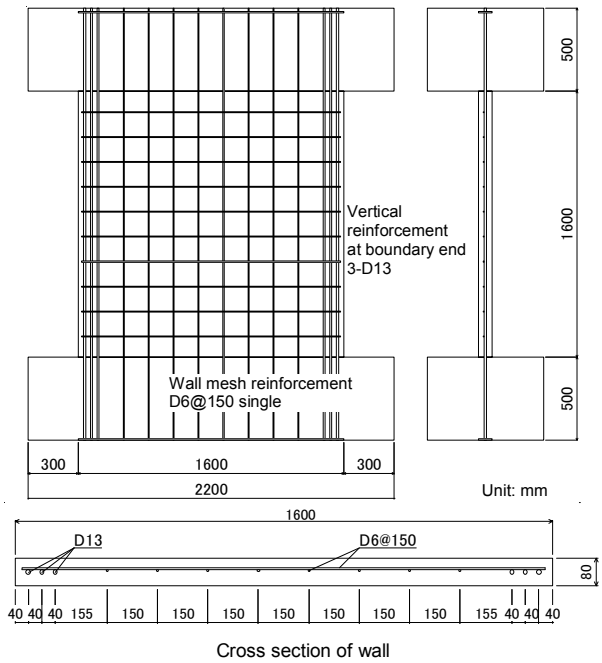

Fig. 2. Bar arrangement (common to all test specimens).

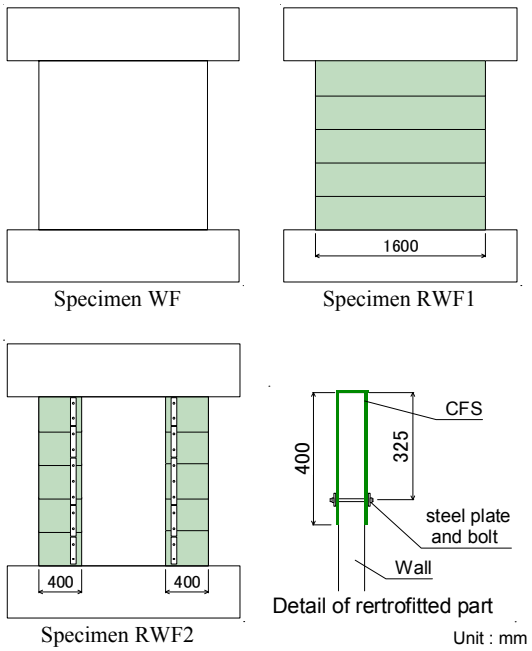

Fig. 3. Schematic diagram of the test specimens.

CFS retrofitting and the extent of retrofitting. Note that all three specimens were walls designed for flexural failure. And wall mesh reinforcement of D6 steel bars used in this test was fabricated with binding wire. Specimen WF represents the unretrofitted test specimen for understanding the basic behavior of the walls. Specimen RWF1 was retrofitted over the entire wall span while specimen RWF2 was partially retrofitted at the boundary ends of the wall as shown in **Fig. 3**.

To attach the CFS, the corners of the walls were chamfered to a diameter of 24 mm, epoxy resin was first applied to the wall surface, the CFS was then attached while maintaining tension manually and with a roller, and then epoxy resin was further applied on top with a roller to impregnate the CFS. Moreover, the top and bottom sheets were overlapped by 12.5 mm each. For specimen RWF2, the CFS was fixed by steel plates (PL-4.5) and threaded bolts (M10). The threaded bolts were installed into drilled hole after concrete casting. And threaded bolts were tightened without management of tightening torque of bolts.

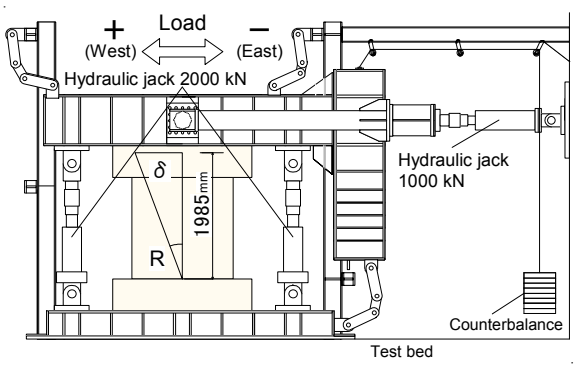

Fig. 4. Description of loading apparatus.

2.2. Loading Program

A description of the loading device is presented in **Fig. 4**. A horizontal lateral force applied in cycles over the positive and negative directions was used for the loading. Also, a constant axial load ($N = 0.08 l_w t_w F_c$) of 343 kN was applied at the top of the specimen using a couple of vertical hydraulic jacks. Where, used F_c of compressive strength of concrete was 33.5 N/mm^2 in this calculation.

Additional moment was applied at the top of the specimen by controlling these vertical jacks to correspond to the acting shear force, such that the shear span ratio was 1.5, using the following equations.

$$N_e = \frac{N}{2} - \frac{Q}{l}(h_s - a), \quad N_w = \frac{N}{2} + \frac{Q}{l}(h_s - a) \quad (1)$$

where, N_e: axial force of east side jack, N_w: axial force of west side jack, N: constant axial force, Q: lateral load, l: distance between two vertical jacks, h_s: assumed height of applied lateral load, and a: actual height of applied lateral load.

In the experiment, the horizontal displacement δ measured at the top stub, divided by the height of the measurement point h (1985 mm), was controlled through the drift angle of the member $R = \delta/h$. The loading cycle started with one cycle of $R = 1/800$ rad, and then two cycles each of $R = 1/400, 1/200, 1/133, 1/100, 1/67, 1/50$ and $1/33$ rad.

2.3. Measuring Method

In the tests, the horizontal displacement was measured, along with the longitudinal deformation at the boundary end of wall and partial deformation of the wall panel. The strains on the longitudinal, horizontal bars of the wall and CFS were measured using strain gages. Additionally, the widths of cracks were measured using a crack scale at each loading cycle.

3. Test Results

3.1. Failure Behavior and the Relationship Between Lateral Load and Drift Angle

The relationship between lateral load and drift angle for each specimen is given in **Fig. 5**. Also, **Fig. 6** shows the

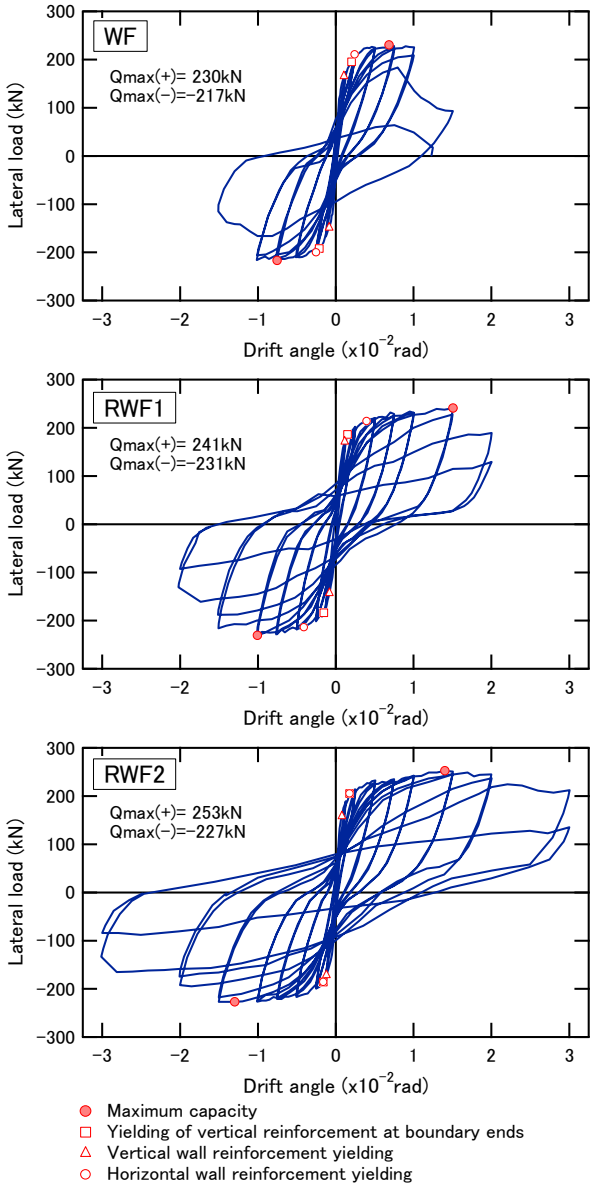

Fig. 5. Lateral load and drift angle relationship.

condition at failure at the wall base for each specimen.

For specimen WF, shear cracks appeared at the same time that the vertical wall reinforcement yielded under the $R = 1/800$ rad cycle, while the horizontal wall reinforcement and the vertical reinforcement at boundary ends yielded under the $R = 1/400$ rad cycle. Afterwards, maximum capacity was reached at the $R = 1/133$ rad cycle; large concrete spalling at the lower part of the wall occurred under the $R = 1/67$ rad cycle, at which point the axial load could not be sustained and loading was terminated (**Fig. 6(a)**).

For specimen RWF1, the vertical wall reinforcement yielded under the $R = 1/800$ rad cycle while the vertical reinforcement at boundary ends yielded under the $R = 1/400$ rad cycle, similar to specimen WF. The horizontal wall reinforcement were found to yield at the $R = 1/200$ rad cycle. Afterwards, maximum capacity was reached at the $R = 1/67$ rad cycle; at the $R = 1/50$ rad cy-

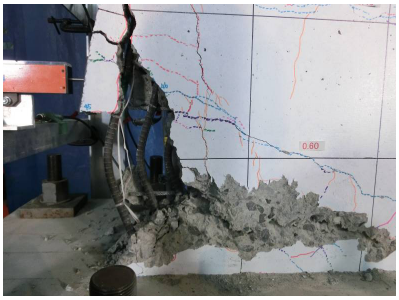

(a) Specimen WF (R = 1/67 rad)

(b) Specimen RWF1 (R = 1/50 rad)

(c) Specimen RWF2 (R = 1/50 rad)

Fig. 6. Wall base condition at failure for each specimen.

cle, concrete swelling at the wall base grew (**Fig. 6(b)**) until swelling occurred at the center of the lower part of the wall as well.

For specimen RWF2, the vertical wall reinforcement yielded under the $R = 1/800$ rad cycle while the horizontal wall reinforcement and the vertical reinforcement at boundary ends yielded under the $R = 1/400$ rad cycle, similar to specimen WF. Afterwards, maximum capacity was reached at the $R = 1/67$ rad cycle; large concrete spalling at the base occurred during the $R = 1/33$ rad cycle. And then, right after commencing with the $R = 1/25$ rad cycle, the axial load could not be sustained and loading was terminated. Looking at the condition at the base during $R = 1/50$ rad, it was found that the swelling was not as much as that of specimen RWF1 (**Fig. 6(c)**).

3.2. The Ultimate Limit Deformation

The envelope curves of the lateral load and drift angle relationship and the ultimate limit deformation angles are plotted in **Fig. 7**. The ultimate limit drift angle was calculated as the drift angle when the strength capacity drops to 90% of maximum capacity.

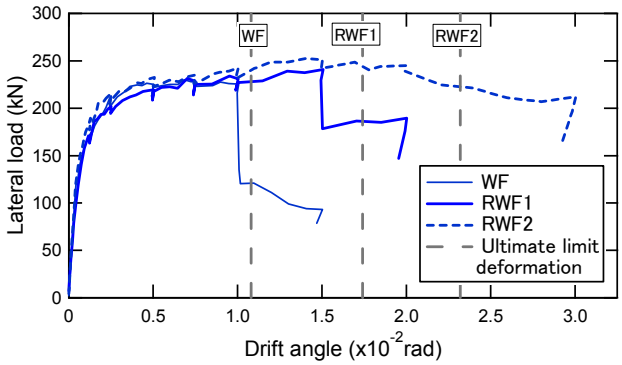

Fig. 7. Envelope curve of lateral load and drift angle.

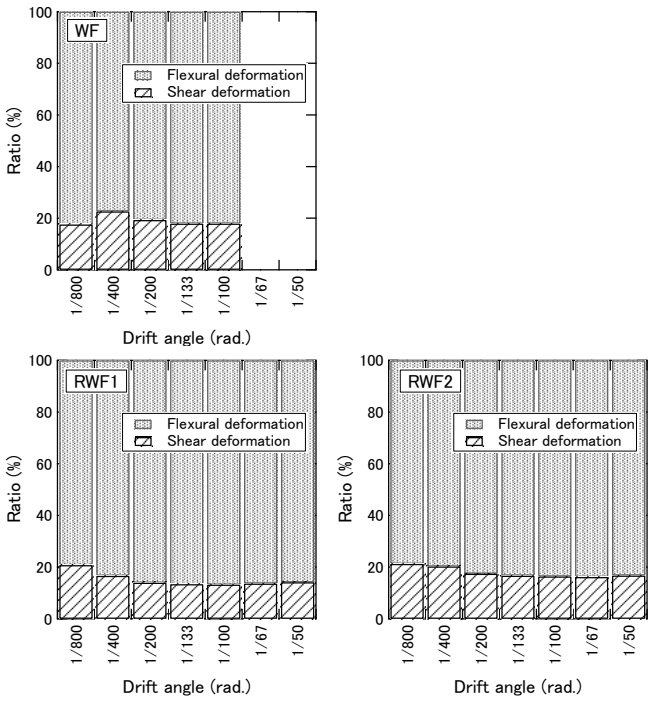

Fig. 8. Ratio of flexural to shear deformation.

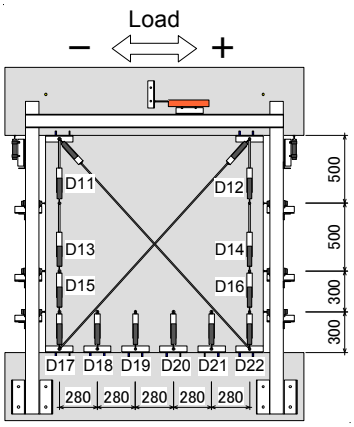

Fig. 9. Displacement gauge measurement points.

Comparing all the specimens, post-maximum strength deterioration for specimens RWF1 and RWF2 were gradual compared to specimen WF although their maximum strength capacity were all at about the same level. It is

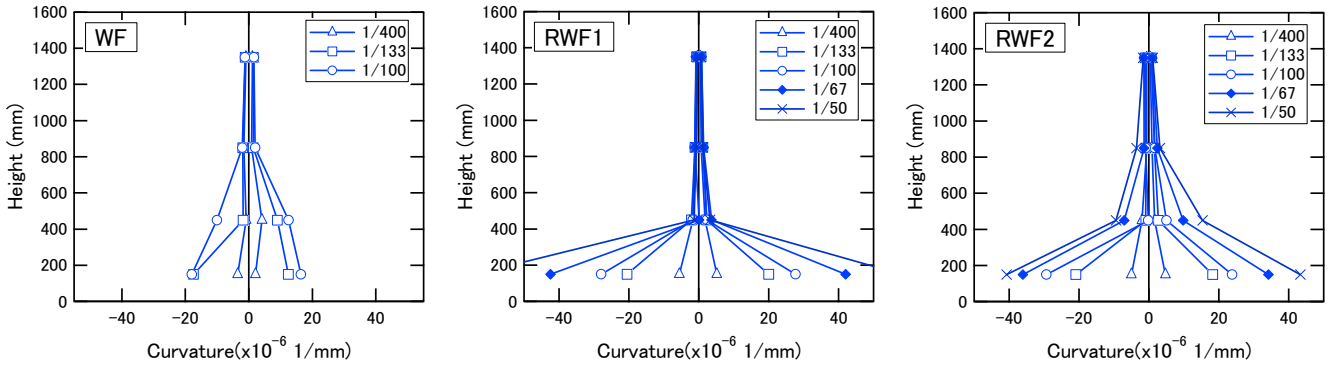

Fig. 10. Curvature distribution.

confirmed that there was an improvement in the deformation performance. The ultimate limit deformation of specimen RWF2 was lager than that of specimen RWF1. It is thought that this difference is caused by confining effect in out of plane direction due to threaded bolts in specimen RWF2.

3.3. Deformation Component

Figure 8 shows the ratio of flexural to shear deformation at the time of positive peak loading. As shown in **Fig. 9**, the wall was divided into 4 sections over its height and the amount of displacements measured at each section. From these displacements, the average curvature was obtained for each section assuming a planar surface was kept. The flexural deformation was then calculated as the sum of these lateral deformations of curvature. The shear deformation was calculated as the lateral displacement minus the flexural deformation.

For all specimens, flexural deformation maintained a ratio of about 80% of the total, accounting for much of the overall deformation. Moreover, shear deformation of specimen RWF1 and RWF2 which were retrofitted specimen was slightly smaller than that of non retrofitted specimen WF.

3.4. Curvature Distribution

The curvature distribution during the first-cycle peak of each cycle is presented in **Fig. 10**. In specimen WF, an overall increasing trend for the curvature could be seen as the loading progressed. As for specimens RWF1 and RWF2, an increasing trend for the wall base curvature could be seen as the loading progressed. It is thought that the crack opening concentrated to the wall base near critical section because CFS adhered to the wall panel could resist to tensile force. And it is found that the number of crack of retrofitted specimen RWF2 is less than that of non retrofitted specimen WF as shown in **Fig. 11** of cracking patterns of specimen WF and specimen RWF2.

3.5. Deformation Distribution at the Wall Base

Figure 12 shows the wall base deformation distribution at the positive peak loading (displacements D17–D22 in

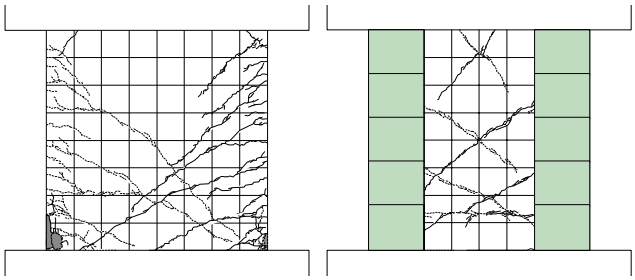

(a) Specimen WF (b) Specimen RWF2

Fig. 11. Cracking patterns ($R = 1/100$ rad).

Fig. 9). Note that measurements from displacement gauge D20 shown in **Fig. 9** for specimen RWF1 could not be get due to an instrument malfunction.

For all the specimens, an increasing trend for the wall base deformation could be seen as the loading progressed. Furthermore, for specimens RWF1 and RWF2, displacements were around twice that of specimen WF. This may be attributed to resisting to tensile force due to CFS in the wall panel, which caused the deformation to concentrate at the wall base as shown in **Fig. 10**. Moreover, the displacements were found to be linearly distributed for all the specimens, confirming that the wall maintained a planar surface.

3.6. CFS Strain

Figure 13 indicates the CFS strain for specimens RWF1 and RWF2. The locations of the strain gauges are illustrated in **Fig. 14**.

According to reference [4], experiments of retrofitted walls have shown that the peak strain of the CFS during maximum strength is about 2000 μ. Specimens picked up in the reference were I-shaped walls which had boundary columns, and failure mode of these specimens were shear failure or slip failure of wall panel. Although the test specimens in the present experiment are not comparable since they were designed for flexural failure, strains between 2000 μ to 3000 μ during maximum capacity have been measured at the wall base even in this experiment, confirming the confining effect of the CFS. Furthermore, strain at the wall center was confirmed to increase starting

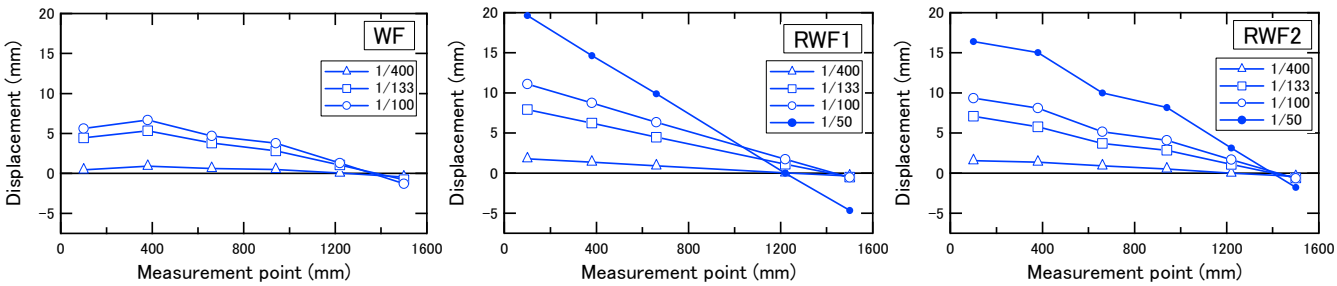

Fig. 12. Wall base deformation distribution.

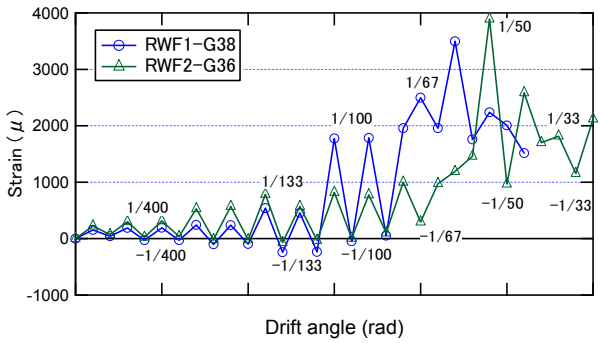

(a) Boundary ends of the wall base

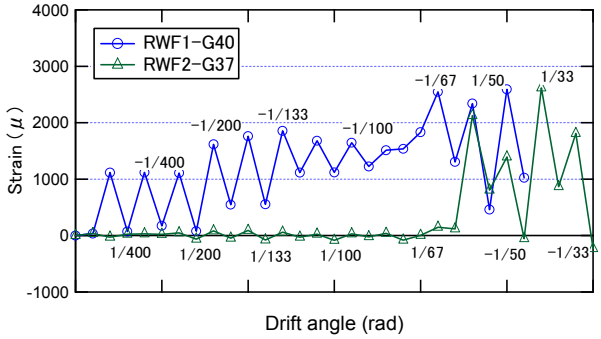

(b) Boundary ends of the wall base

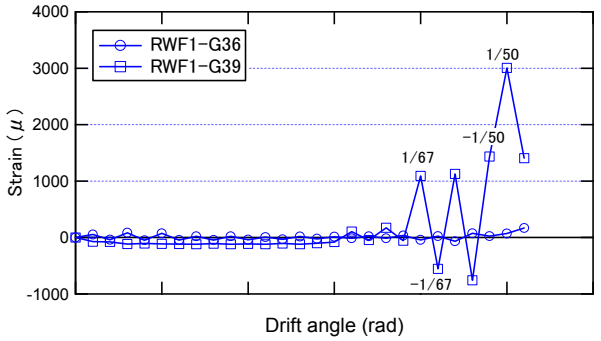

(c) Middle area of wall

Fig. 13. CFS strain.

from the $R = 1/67$ rad cycle, when concrete crushing has advanced as shown in **Fig. 13(c)**.

4. Evaluation of Ultimate Bearing Capacity

The results of the bearing capacity calculations for the specimens are shown in **Table 5**. Using reference [5] for the bearing capacity of the specimens, the flexural and

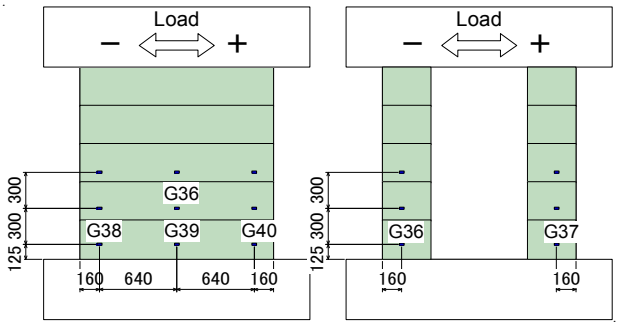

Fig. 14. Strain gauge locations.

Table 5. Bearing capacity calculation results.

Specimen	WF	RWF1	RWF2
Q_{mu} (kN)	212	212	212
Q_{su} (kN)	341	349	325
Experimental value (kN)	230	241	253
Experimental value $/Q_{mu}$	1.08	1.14	1.20

shear strength were calculated using the following equations. The effect of CFS was not considered in these calculations.

$$M_{wu} = a_t \sigma_y l_w + 0.5 a_w \sigma_{wy} l_w + 0.5 N l_w \quad . \quad . \quad . \quad . \quad (2)$$

where, a_t: total cross-sectional area of the vertical reinforcement at boundary ends on the tensile side (mm^2), σ_y: yield strength of the vertical reinforcement at boundary ends on the tensile side (N/mm^2), l_w: $0.9D$ (mm), a_w: cross-sectional area of the vertical wall reinforcement (mm^2), σ_{wy}: yield strength of the vertical wall reinforcement (N/mm^2), N: axial force on the wall (N)

$$Q_{su} = \left[\frac{0.068 p_{te}^{0.23} \cdot (F_c + 18)}{\sqrt{M/(Q \cdot d) + 0.12}} + 0.85\sqrt{\sigma_{wh} \cdot p_{wh}} + 0.1\sigma_0 \right] \cdot t_e \cdot j \quad (3)$$

where, p_{te}: equivalent tensile reinforcement ratio (%), F_c: concrete strength (N/mm^2), M/Qd: shear span ratio, σ_{wh}: yield strength of the horizontal wall reinforcement (N/mm^2), p_{wh}: horizontal wall reinforcement ratio with t_e as thickness, σ_0: average axial stress with respect to

the total cross-sectional area (N/mm^2), t_e: wall thickness (mm), and j: 7/8d (mm).

Looking at the calculation results, the value of the experimental maximum capacity is greater than the value of the flexural strength. Moreover, a good correspondence was confirmed, with the ratio of the experimental value to the calculated value of the flexural strength shown to be ranging between 1.08–1.20.

5. Conclusions

An experimental study was conducted on RC shear walls without boundary columns retrofitted by CFS, where the following findings were obtained.

By retrofitting the RC shear wall without boundary columns with CFS, post-maximum strength deterioration was more gradual, confirming the improvement in deformation performance.

Ultimate limit deformation of specimen which was partially retrofitted at the boundary ends of the wall was larger than that of specimen which was retrofitted over the entire wall span.

CFS strains were between 2000 μ to 3000 μ during maximum capacity, confirming the confining effect of the CFS.

The flexural strength of the specimens of RC shear wall without boundary columns retrofitted with CFS can be evaluated using existing formulas.

Acknowledgements

This study was conducted with a grant from the "Enhancement of Earthquake and Tsunami Disaster Mitigation Technology in Peru" (Principal Investigator: Prof. Fumio Yamazaki, Chiba University), a project of the Science and Technology Research Partnership for Sustainable Development (SATREPS) program, a collaboration of JST (Japan Science and Technology Agency) and JICA (Japan International Cooperation Agency). Also, the authors would like to acknowledge the contribution of Toray Industries, Inc., by providing materials and technical guidance during the making of the retrofit specimens. We take this opportunity to express our appreciation.

References:

[1] C. Zavala, P. Gibu, L. Lavado, J. Taira, L. Cardenas, and L. Ceferino, "Cyclic Behavior of Low Ductility Walls Considering Perpendicular Action," Journal of Disaster Research, Vol.8, No.2, pp. 312-319, 2013.

[2] Architectural Institute of Japan, "Reconnaissance Report of The 2010 Chile Off Maule Earthquake," 2012.

[3] K. Horie, Y. Matsuzaki, H. Fukuyama, M. Iso, N. Yoshida, and N. Hayashida, "A Study on Retrofitting of Shear Wall with Continuous Fiber Sheet," Summaries of technical papers of the Annual Meeting, Architectural Institute of Japan, pp. 595-600, 1997 (in Japanese).

[4] Japan Building Disaster Prevention Association, "2010 revised edition, Guidelines for the Earthquake-resistant Renovation Design and Construction of Existing RC and SRC Buildings Using Continuous Fiber Sheets," 2010 (in Japanese).

[5] Building Center of Japan, "2007 edition, Manual of Technical Standards Related to the Structure of Buildings," 2007 (in Japanese).

Name:
Tomoya Matsui

Affiliation:
Associate Professor, Toyohashi University of Technology

Address:
1-1 Hibarigaoka, Tenpaku, Toyohashi, Aichi 441-8580, Japan

Brief Career:
2005-2005 Research Associate, Toyohashi University of Technology
2005-2012 Assistant Professor, Toyohashi University of Technology
2012- Associate Professor, Toyohashi University of Technology

Selected Publications:
• T. Matsui, S. Suzuki, and H. Kuramoto, "Experimental Study on Structural Performance of Precast CES Shear Walls," Proc. of fifteenth World Conf. on Earthquake Engineering (15thWCEE), No.2177, 2012.
• T. Matsui and H. Kuramoto, "Structural Performance and FEM Analysis of CES Beam-Column Joints," Proc. of 10th Int. Conf. on Advances in Steel Concrete Composite and Hybrid Structures (ASCCS2012), pp. 733-740, 2012.

Academic Societies & Scientific Organizations:
• Architectural Institute of Japan (AIJ)
• Japan Concrete Institute (JCI)
• Japan Associate for Earthquake Engineering (JAEE)